

# Tracing the origin of the oxygen-consuming organic matter in the hypoxic zone in a large eutrophic estuary: the lower reach of the Pearl River Estuary, China

Jianzhong Su<sup>1</sup>, Minhan Dai<sup>1\*</sup>, Biyan He<sup>1,2</sup>, Lifang Wang<sup>1</sup>, Jianping Gan<sup>3</sup>, Xianghui Guo<sup>1</sup>, Huade Zhao<sup>1</sup> and Fengling Yu<sup>1</sup>

<sup>1</sup>State Key Laboratory of Marine Environmental Science, Xiamen University, Xiamen, China

<sup>2</sup>College of Food and Biological Engineering, Jimei University, Xiamen, China

<sup>3</sup>Department of Mathematics and Division of Environment, Hong Kong University of Science and Technology, Kowloon, Hong Kong, China

\*Correspondence to: Minhan Dai (mdai@xmu.edu.cn)

**Abstract.** We assess the relative contributions of different sources of organic matter, marine vs. terrestrial, to oxygen consumption in an emerging hypoxic zone in the lower Pearl River Estuary (PRE), a large eutrophic estuary located in Southern China. Our cruise, conducted in July 2014, consisted of two legs before and after the passing of Typhoon Rammasun, which completely de-stratified the water column. The stratification recovered rapidly, within one day after the typhoon. We observed algal blooms in the upper layer of the water column and hypoxia underneath in bottom water during both legs. Repeat sampling at the initial hypoxic station showed severe oxygen depletion down to  $30 \mu\text{mol kg}^{-1}$  before the typhoon and a clear drawdown of dissolved oxygen after the typhoon. Based on a three end-member mixing model and the mass balance of dissolved inorganic carbon and its isotopic composition, the  $\delta^{13}\text{C}$  of organic carbon remineralized in the hypoxic zone was  $-23.2 \pm 1.1 \text{ ‰}$ . We estimated that  $65 \pm 16 \%$  of the oxygen-consuming organic matter was derived from marine sources, and the rest ( $35 \pm 16 \%$ ) was derived from the continent. In contrast to a recently studied hypoxic zone in the East China Sea off the Changjiang Estuary where marine organic matter stimulated by eutrophication dominated oxygen consumption, here terrestrial organic matter significantly contributed to the formation and maintenance of hypoxia. How varying amounts of these organic matter sources drive oxygen consumption has important implications for better understanding hypoxia and its mitigation in bottom waters.

## 1 **1 Introduction**

2 The occurrence of hypoxia has been exacerbated worldwide (Nixon, 1995; Diaz and  
3 Rosenberg, 2008; Rabalais et al., 2010; Zhang et al., 2013). In recent decades, more  
4 than 400 coastal hypoxic systems have been reported with an exponential growth rate  
5 of  $5.5 \pm 0.23$  % yr<sup>-1</sup>, demonstrating their persistence and complexity with respect to both  
6 science and management (Diaz and Rosenberg, 2008; Vaquer-Sunyer and Duarte,  
7 2008). Hypoxia may not only reduce biodiversity and endanger aquatic and benthic  
8 habitats, but also alter the redox chemistry in both the water column and the underlying  
9 sediments, triggering the release of secondary pollutants (Breitburg, 2002; Rutger et  
10 al., 2002). Moreover, the management and recovery of these systems is complicated  
11 due to the hysteresis of hypoxic conditions, and the varying timescales of biological  
12 loss (within hours to weeks) and recovery from hypoxia (from months to years)  
13 (Steckbauer et al., 2011).

14 Coastal hypoxia usually occurs in stratified water columns where the downward  
15 mixing of oxygen from the surface is impeded (Kemp et al., 2009). Below the  
16 pycnocline, aerobic respiration is usually the predominant sink of oxygen. Organic  
17 matter, which consumes dissolved oxygen (DO) as it becomes oxidized, is thus the  
18 ultimate cause of hypoxia under favourable physical settings (Rabouille et al., 2008;  
19 Rabalais et al., 2014; Qian et al., 2016). The organic carbon (OC) that fuels  
20 respiration-driven reduction of oxygen in these systems could originate from either  
21 eutrophication-induced primary production (marine OC; OC<sub>mar</sub>), or naturally and/or  
22 anthropogenically driven delivery from terrestrial environments (terrestrial OC; OC<sub>terr</sub>)  
23 (Paerl, 2006; Rabalais et al., 2010).

24 The question of how much OC in hypoxic zones is supplied from on-site primary  
25 production versus the quantity derived from terrestrial sources has been an issue of  
26 debate (Wang et al., 2016). Much of the phytoplankton-centric hypoxia literature  
27 suggests that OC<sub>mar</sub> dominates oxygen consumption in hypoxic zones, owing to its  
28 higher microbial availability than OC<sub>terr</sub> (Zimmerman and Canuel, 2000; Boesch et al.,  
29 2009; Carstensen et al., 2014). Wang et al. (2016) quantified for the first time the  
30 relative contributions of particulate OC<sub>mar</sub> (POC<sub>mar</sub>) and particulate OC<sub>terr</sub> (POC<sub>terr</sub>) in  
31 consuming DO in the bottom waters of the East China Sea (ECS) off the Changjiang  
32 Estuary (CJE), and found that POC<sub>mar</sub> dominated DO consumption. However, other  
33 studies suggest that POC<sub>terr</sub> may also play an important role (Swarzenski et al., 2008;

1 Bianchi, 2011a; Bianchi et al., 2011b). It is thus very important to quantify the relative  
2 contributions of organic matter ( $OC_{\text{mar}}$  vs.  $OC_{\text{terr}}$ ) driving the onset and maintenance of  
3 hypoxia in coastal systems, since reducing organic matter vs. nutrient inputs requires a  
4 different set of management strategies.

5 The Pearl River Estuary (PRE, 21.2 °N–23.1 °N, 113.0 °E–114.5 °E) is surrounded  
6 by several large cities including Hong Kong, Shenzhen and Guangzhou and has  
7 received very high loads of nutrients from the drainage basin in the last three decades.  
8 As such, eutrophication has increasingly become an issue of concern (Huang et al.,  
9 2003; Ye et al., 2012). Dissolved inorganic nitrogen (DIN) concentrations in the PRE  
10 have increased approximately 4-fold from 1986 (19.3  $\mu\text{mol L}^{-1}$ ) to 2002 (76.1  $\mu\text{mol}$   
11  $\text{L}^{-1}$ ) (He and Yuan, 2007). This DIN increase has been attributed to increased inputs of  
12 domestic sewage, industrial wastewater, agricultural runoff and aquaculture in the  
13 watershed (Huang et al., 2003).

14 Recent observations based on monthly surveys between April 2010 and March 2011  
15 and long term monitoring data from 1990 to 2014, have suggested that the lower PRE  
16 has emerged as a seasonal hypoxic zone (Qian et al., 2017). This is supported by our  
17 current study, as two relatively large hypoxic zones ( $> 300 \text{ km}^2$ ) were observed in the  
18 lower PRE with  $\text{DO} < 2 \text{ mg L}^{-1}$ . However, the origin of the organic matter driving  
19 hypoxia in the lower PRE has not previously been examined. Here, we quantified the  
20 relative proportions of  $OC_{\text{mar}}$  and  $OC_{\text{terr}}$  contributing to DO drawdown in bottom waters  
21 of the lower PRE, an economically important coastal region. This study has important  
22 biological, societal and managerial implications for the region, particularly relating to  
23 water quality in the vicinity of Hong Kong in the lower PRE. For example, the  
24 government of Hong Kong is examining the efficacy of its costly Harbour Area  
25 Treatment Scheme project and if additional treatment should be implemented  
26 (<http://www.gov.hk/en/residents/environment/water/harbourarea.htm>).

## 27 **2 Materials and Methods**

### 28 **2.1 Sampling and analysis**

29 Interrupted by Typhoon Rammasun on 17-18 July 2014, our cruise was divided into  
30 two legs (Fig. 1). During Leg 1 on 13–16 July, we sampled Transects F4, F5 and  
31 Stations A08–A18. During Leg 2 on 19–27 July, we sampled Stations A01–A10,  
32 Transects F3 and F4, Stations A11–A17 and Transects F5, F6, F1, and F2, in sequence.

1 In order to monitor the development of hypoxia before and after the passage of the  
2 typhoon, we revisited Station A10 three more times (13, 20 and 27 July).

3 According to the gauge in the upper Pearl River, water discharge peaked in June and  
4 July. Typhoon Rammasun increased discharge during 15-18 July, with daily average  
5 values of 19480, 26115, 22981 and 17540 m<sup>3</sup> s<sup>-1</sup>, respectively. Nevertheless, the  
6 freshwater discharge was 18908 m<sup>3</sup> s<sup>-1</sup> in leg 1 and 15698 m<sup>3</sup> s<sup>-1</sup> in leg 2, comparable  
7 to the long-term (2000–2011) monthly average.

8 Temperature and salinity were determined with a SBE 25  
9 Conductivity-Temperature-Depth/Pressure unit (Sea-Bird Co.). Water samples were  
10 collected using 4 L Go-Flo bottles (General Oceanics). DIC and DO was measured at  
11 all stations with depth profiles. Samples for  $\delta^{13}\text{C}_{\text{DIC}}$  were collected primarily along  
12 Transect A as well as at depth in low oxygen layers.

13 The DO concentrations in discrete water samples were measured on board within 8 h  
14 using the classic Winkler titration method (Dai et al., 2006). In addition, we conducted  
15 on-deck incubation experiments using unfiltered water taken from the hypoxic zone  
16 on 27 July, 2014 following He et al. (2014). Bottom water from ~2 m above the  
17 sediment surface was collected and incubated for 24 hours in 65 mL BOD bottles in  
18 dark at ambient temperature controlled by the flowing surface water. Total oxygen  
19 consumption rate was determined by comparing the DO concentration at the initial  
20 and end point of the experiment.

21 DIC was measured with an infrared detector after acidifying 0.5–0.7 mL of water  
22 sample with a precision of 0.1 % for estuarine and sea waters (Cai et al., 2004).  
23 Dissolved calcium concentrations ( $\text{Ca}^{2+}$ ) were determined using an EGTA titration  
24 with a Metrohm 809 TITRANDO potentiometer, which has a precision better than  $\pm 5$   
25  $\mu\text{mol kg}^{-1}$  (Cao et al., 2011).

26 For  $\delta^{13}\text{C}_{\text{DIC}}$  analysis, an ~20 mL DIC sample was converted into gaseous  $\text{CO}_2$  and  
27 progressively purified through a vacuum line. The pure  $\text{CO}_2$  sample was analyzed with  
28 an isotope ratio mass spectrometer (IRMS, Finnigan MAT 252, Bremen, Germany).  
29 The analytical precision was better than 0.1 ‰.

30 Water samples for TSM (total suspended matter), POC and  $\delta^{13}\text{C}_{\text{POC}}$  analysis were  
31 concentrated onto preweighed and pre-combusted 0.7  $\mu\text{m}$  Whatman GF/F filters after  
32 filtering 0.2–1.0 L of water under a mild vacuum (~ 25 kPa). Filters were washed with  
33 distilled water and stored at -20 °C. Prior to analysis, all filters were freeze-dried. TSM

1 was determined using the net weight increment on the filter and the filtration volume.  
 2 Filters were decarbonated with 1.0 mol L<sup>-1</sup> HCl and dried at 40 °C for 48 h (Kao et al.,  
 3 2012) and analyzed for POC and  $\delta^{13}\text{C}_{\text{POC}}$  on an elemental analyzer coupled with an  
 4 IRMS (EA-IRMS). The analytical precision for  $\delta^{13}\text{C}_{\text{POC}}$  was better than 0.1 ‰. Chl-a  
 5 was measured with a Turner fluorometer after extracting filters with 90 % acetone (He  
 6 et al., 2010b). Calibrations were performed using a Sigma Chl-a standard.

## 7 **2.2 Three end-member mixing model**

8 We adopted a three end-member mixing model to construct the conservative mixing  
 9 scheme among different water masses (Cao et al., 2011; Han et al., 2012):

$$10 \quad F_{\text{RI}} + F_{\text{SW}} + F_{\text{SUB}} = 1 \quad (1)$$

$$11 \quad \theta_{\text{RI}} \times F_{\text{RI}} + \theta_{\text{SW}} \times F_{\text{SW}} + \theta_{\text{SUB}} \times F_{\text{SUB}} = \theta \quad (2)$$

$$12 \quad S_{\text{RI}} \times F_{\text{RI}} + S_{\text{SW}} \times F_{\text{SW}} + S_{\text{SUB}} \times F_{\text{SUB}} = S \quad (3)$$

13 where  $\theta$  and  $S$  represent potential temperature and salinity; the subscripts RI, SW, and  
 14 SUB denote the three different water masses (Pearl River plume water, offshore surface  
 15 seawater and upwelled subsurface water); and  $F_{\text{RI}}$ ,  $F_{\text{SW}}$ , and  $F_{\text{SUB}}$  represent the  
 16 fractions that each end-member contributes to the in situ samples. These fractions were  
 17 applied to predict conservative concentrations of DIC ( $\text{DIC}_{\text{con}}$ ) and its isotopic  
 18 composition ( $\delta^{13}\text{C}_{\text{DICcon}}$ ) resulting solely from conservative mixing.

$$19 \quad \text{DIC}_{\text{RI}} \times F_{\text{RI}} + \text{DIC}_{\text{SW}} \times F_{\text{SW}} + \text{DIC}_{\text{SUB}} \times F_{\text{SUB}} = \text{DIC}_{\text{con}} \quad (4)$$

$$20 \quad \frac{\delta^{13}\text{C}_{\text{DICRI}} \times \text{DIC}_{\text{RI}} \times F_{\text{RI}} + \delta^{13}\text{C}_{\text{DICSW}} \times \text{DIC}_{\text{SW}} \times F_{\text{SW}} + \delta^{13}\text{C}_{\text{DICSUB}} \times \text{DIC}_{\text{SUB}} \times F_{\text{SUB}}}{\text{DIC}_{\text{con}}} = \delta^{13}\text{C}_{\text{DICcon}} \quad (5)$$

21 The difference ( $\Delta$ ) between measured and conservative DIC values represents the  
 22 magnitude of the biological alteration of DIC (Wang et al., 2016).

## 23 **3 Results**

### 24 **3.1 Horizontal distribution**

25 Although the average freshwater discharge rate during our sampling period (16369 m<sup>3</sup>  
 26 s<sup>-1</sup>) was slightly higher than the multi-year (2000–2011) monthly average (15671 m<sup>3</sup>  
 27 s<sup>-1</sup>), typhoon Rammasun modified the system to some extent as shown from the  
 28 evolution of chemical species at Station A10 before and after the typhoon (See Sect.  
 29 3.4). The interruption of Leg 1 due to the typhoon (July 17-18) led to a smaller survey  
 30 area, covering only outside Lingdingyang Bay (traditionally regarded as the PRE),

1 while Leg 2 covered Lingdingyang Bay from the Humen Outlet to the adjacent coastal  
2 sea.

3 As depicted in Fig. 2, the sea surface temperature (SST) during Leg 1 (28.9-32.2 °C)  
4 was slightly higher than during Leg 2 (28.9-31.0 °C). Sea surface salinity (SSS)  
5 measurements showed that plume water was restricted more landward during Leg 2  
6 than Leg 1. However, a steeper gradient to higher SST offshore during Leg 1 was  
7 likely induced by the upwelling of bottom water, featuring relatively high SSS (18.6),  
8 high DIC (1789  $\mu\text{mol kg}^{-1}$ ) and low DO saturation (DO%, 86 %). During Leg 1, the  
9 region with the most productivity was found east of the Wanshan Islands, characterized  
10 by high concentrations of Chl-a (8.0  $\mu\text{g kg}^{-1}$ ), low concentrations of DIC (1607  $\mu\text{mol}$   
11  $\text{kg}^{-1}$ ), and DO supersaturation, with the highest DO% greater than 160 % at Station  
12 F503. During Leg 2, there were three patches of high productivity, south of  
13 Huangmaohai, at the PRE entrance, and off Hong Kong. The central region of high  
14 productivity had the highest DO%, greater than 140% at Station A14, and was  
15 characterized by relatively high concentrations of Chl-a (7.8  $\mu\text{g kg}^{-1}$ ) and low  
16 concentrations of DIC (1737  $\mu\text{mol kg}^{-1}$ ).

17 As shown in Fig. 3, bottom water hypoxia during Leg 1 was located more centrally in  
18 the study area relative to the surface phytoplankton bloom. The center of the hypoxic  
19 zone was found at Station A10, characterized by the lowest observed DO  
20 concentrations (as low as 30  $\mu\text{mol kg}^{-1}$ ) and a relatively high concentration of DIC  
21 (2075  $\mu\text{mol kg}^{-1}$ ). During Leg 2, hypoxic conditions were no longer found at Station  
22 A10, and instead the largest hypoxic zone was discovered to the southwest of the  
23 Wanshan Islands, where the lowest DO values were observed (as low as 7  $\mu\text{mol kg}^{-1}$  at  
24 F304), and once again coincided with relatively high concentrations of DIC (2146  $\mu\text{mol}$   
25  $\text{kg}^{-1}$ ). We were unable to precisely constrain the areas of the regions impacted by  
26 bottom water hypoxia due to the limited spatial coverage, but our results suggest it  
27 covered an area of  $> 280 \text{ km}^2$  during Leg 1 and  $> 290 \text{ km}^2$  during Leg 2 according to  
28 the definition of hypoxia as  $\text{DO} < 2 \text{ mg L}^{-1}$  or 63  $\mu\text{M}$ , or an area of  $> 900 \text{ km}^2$  during  
29 Leg 1 and  $> 800 \text{ km}^2$  during Leg 2 assuming the threshold of the oxygen-deficit zone  
30 was  $< 3 \text{ mg L}^{-1}$  or 95  $\mu\text{M}$  (Rabalais et al., 2010; Zhao et al., 2017).

## 1 **3.2 Vertical distribution**

2 During Leg 1, plume water reached 50 km offshore from the entrance of the PRE,  
3 forming a 5–10 m thick surface layer (Fig. 4b). Both the thermocline and halocline  
4 contributed to the stability of the water column structure, which favored the formation  
5 of bottom water hypoxia. The thickness of the bottom water hypoxic layer was ~ 5 m.  
6 The region of highest productivity, however, was not observed in the same location as  
7 the hypoxic zone, but further offshore.

8 During Leg 2, although the passing of the typhoon would be expected to absorb large  
9 amounts of potential heat and cause extensive mixing of the water column, the  
10 enhanced freshwater discharge could rapidly re-stratify the water column and facilitate  
11 the re-formation of hypoxia. This time, the primary region of hypoxia was observed  
12 directly below the bloom, with a thickness of 3 m (Fig. 4i). Additionally, near the  
13 Humen Outlet we observed low DIC ( $1466 \mu\text{mol kg}^{-1}$ ) and moderately low DO ( $89$   
14  $\mu\text{mol kg}^{-1}$ ), which reflected the input of the low DO water mass from upstream as  
15 reported previously (Dai et al., 2006; Dai et al., 2008a; He et al., 2014).

## 16 **3.3 Isotopic composition of DIC and POC**

17 The  $\delta^{13}\text{C}$  values of DIC became progressively heavier from stations dominated by  
18 freshwater ( $\sim -11.4 \text{ ‰}$ ) to off-shore seawater ( $\sim -0.6 \text{ ‰}$ ), with a relatively wide range of  
19 values beyond a salinity of 13 (Fig. 5). Owing to a malfunction of the instrument,  
20  $\delta^{13}\text{C}_{\text{POC}}$  data from our cruise were not available. Instead, we reported a valid  $\delta^{13}\text{C}_{\text{POC}}$   
21 dataset from a 2015 summer cruise in approximately the same region.  $\delta^{13}\text{C}_{\text{POC}}$  values  
22 showed a similar trend with  $\delta^{13}\text{C}_{\text{DIC}}$ , i.e.  $^{13}\text{C}$  enriched seaward, from  $\sim -28 \text{ ‰}$  to  $\sim -20$   
23  $\text{‰}$ . In the bloom, where the DO% was above 125 %, the mean  $\delta^{13}\text{C}$  value for POC  
24 was  $-19.4 \pm 0.8 \text{ ‰}$  ( $n=8$ ), which was within the typical range of marine phytoplankton  
25 (Peterson and Fry, 1987). As shown in Fig. 5, there was a large  $\delta^{13}\text{C}_{\text{POC}}$  decrease near a  
26 salinity of 15. Geographically, it was located at the mixing dominated zone in inner  
27 Lingdingyang Bay, where intense resuspension of  $^{13}\text{C}$  depleted sediments may occur  
28 (Guo et al., 2009).

## 29 **3.4 Reinstatement of the hypoxic station after Typhoon Rammasun**

30 Typhoon Rammasun made landfall at Zhanjiang, located 400 km to the southwest of  
31 the PRE, at 20:00 LT (Local Time) on 18 July, and was dissipated by 05:00 LT on 20

1 July. The typhoon completely de-stratified the water column during its passing.  
2 However, the associated heavy precipitation and runoff appeared to re-establish  
3 stratification rather quickly, within one day, as suggested by the salinity gradient (18–  
4 30) from 0–10 m depth during Leg 2 at 15:20 LT on 20 July (Fig. 6b). In order to  
5 capture the evolution of DO between the disruption and reinstatement of stratification,  
6 we resumed our cruise and revisited Station A10 (Fig. 6). On 13 July, the bottom water  
7 at Station A10 was the hypoxic core, with the lowest observed DO ( $30 \mu\text{mol kg}^{-1}$ ) and  
8 highest DIC ( $2075 \mu\text{mol kg}^{-1}$ ) concentrations. On 20 July, the results showed that the  
9 temperature homogeneous layer in the bottom water (9–13 m) might reflect the  
10 remnants of typhoon-induced mixing (Fig. 6a), while the reduction in salinity at  $<9$  m  
11 depicted the rapid re-establishment of stratification as a result of enhanced freshwater  
12 discharge (Fig. 6b). Bottom water DO increased to  $153 \mu\text{mol kg}^{-1}$  and DIC decreased to  
13  $1901 \mu\text{mol kg}^{-1}$  as a result of the typhoon-induced water column mixing and aeration. In  
14 addition, TSM increased sharply from 20.2 before the typhoon to  $36.6 \text{ mg kg}^{-1}$ ,  
15 suggesting large volumes of sediment had been resuspended during its passing. On 27  
16 July, one week after the typhoon, strong thermohaline stratification was re-established  
17 in the whole water column. Along with the intensifying stratification, bottom water DO  
18 decreased to  $99 \mu\text{mol kg}^{-1}$  indicating continuous DO depletion and the potential for  
19 hypoxia formation. Meanwhile, bottom water DIC concentrations increased to  $2000$   
20  $\mu\text{mol kg}^{-1}$  and dissolved inorganic phosphate (DIP) rose from 0.28 to  $0.57 \mu\text{mol kg}^{-1}$ .  
21 Moreover, bottom-water TSM returned to pre-typhoon (13 July) levels.

## 22 **4 Discussion**

### 23 **4.1 Selection of end-members and model validation**

24 The potential temperature-salinity plot displayed a three end-member mixing scheme  
25 over the PRE and adjacent coastal waters (Fig. 7a), consisting of Pearl River plume  
26 water, offshore surface seawater and upwelled subsurface water. During the summer, a  
27 DIC concentration of  $\sim 1917 \mu\text{mol kg}^{-1}$  was observed at  $S=33.7$ , which can be regarded  
28 as the offshore surface seawater end-member (Guo and Wong, 2015). Here, by  
29 choosing  $S=34.6$  as the offshore subsurface water salinity end-member, we obtained a  
30 DIC value of  $\sim 2023 \mu\text{mol kg}^{-1}$ , similar to the value at  $\sim 100$  m depth adopted by Guo  
31 and Wong (2015). For the plume end-member, it was difficult to directly select from the



1 field data, because biological alteration might lead to altered values within the plume  
2 influenced area. Therefore, we first assumed that the plume water observed on the shelf  
3 consisted of a mixture of freshwater and offshore surface seawater. Then, we compiled  
4 3 years of surface data from the summer (August 2012, July 2014 and July 2015) to  
5 extrapolate the relatively stable freshwater end-member and examine the biological  
6 effect on DIC-salinity relationships. By constraining DIC end-members (freshwater  
7 and offshore surface seawater), we observed that DIC remained overall conservative  
8 when salinity was  $<10.8$  but showed removal when salinity was  $>10.8$  (Han et al.,  
9 2012). Thus, we derived plume end-member values ( $1670 \pm 50 \mu\text{mol kg}^{-1}$ ) from the  
10 DIC-salinity conservative mixing curve at  $S=10.8$ . Furthermore,  $S=10.8$  was observed  
11 at the innermost station (A08) during Leg 1, which agreed well with the spatial and  
12 temporal scale of the actual water mass mixing in our survey. To confirm our results,  
13 we also used a freshwater end-member ( $S=0$ ), but the output of the model showed little  
14 difference from that based on the plume end-member at  $S=10.8$ .

15 The  $\delta^{13}\text{C}_{\text{DIC}}$  value was  $0.6 \pm 0.2 \text{ ‰}$  in the offshore surface seawater at  $S \sim 33.7$ , where  
16 nutrient ( $\text{NO}_3^- + \text{NO}_2^-$  and DIP) concentrations were close to their detection limits and  
17 DO was nearly saturated, indicating little biological activity. As DIC remained overall  
18 conservative when salinity was  $< 10.8$ , the  $\delta^{13}\text{C}_{\text{DIC}}$  value of  $-11.4 \pm 0.2 \text{ ‰}$  at  $S < 0.4$  is  
19 representative of the freshwater source. Assuming the plume water is a mixture of  
20 freshwater and offshore surface seawater, the initial plume end-member of  $\delta^{13}\text{C}_{\text{DIC}}$  at  
21  $S=10.8$  can be calculated via an isotopic mass balance ( $-7.0 \pm 0.8 \text{ ‰}$ ). A summary of the  
22 end-member values used in this study is listed in Table 1.

23 We calculated the fractions of the three water masses based on potential temperature  
24 and salinity equations, so as to predict conservative DIC ( $\text{DIC}_{\text{con}}$ ) and its isotopic  
25 composition ( $\delta^{13}\text{C}_{\text{DICcon}}$ ) solely from conservative mixing. We chose the concentration  
26 of  $\text{Ca}^{2+}$  as a conservative tracer to validate our model prediction, assuming  $\text{CaCO}_3$   
27 precipitation or dissolution is not significant. This assumption is supported by a strong  
28 linear relationship between surface water  $\text{Ca}^{2+}$  and salinity, and aragonite  
29 oversaturation ( $\Omega_{\text{arag}} = 2.6 \pm 0.7$ ) in the subsurface water. Our model derived values  
30 were in good accordance with the field-observed values (Fig. 7b), which strongly  
31 supported our model prediction.

32 As shown in Fig. 7c, most of the observed DIC concentrations in the subsurface water  
33 were higher than the conservative values, as a result of DIC production via OC

1 oxidation. This coincided with lighter  $\delta^{13}\text{C}_{\text{DIC}}$  values than conservative, owing to the  
 2 accumulation of isotopically lighter carbon entering the DIC pool from remineralized  
 3 organic matter (Fig. 7d). Based on the differences between the observed and  
 4 conservative values of DIC and  $\delta^{13}\text{C}_{\text{DIC}}$ , the carbon isotopic composition of the  
 5 oxygen-consuming organic matter could be traced precisely (see details in Sect. 4.2).

6 In the subsurface water, the bulk of  $\Delta\text{DIC}$  values varied from 0 to 132  $\mu\text{mol kg}^{-1}$ ,  
 7 coupled with a range of apparent oxygen utilization (AOU) values from 0 to 179  $\mu\text{mol}$   
 8  $\text{kg}^{-1}$ .  $\Delta\text{DIC}$  values positively correlated with AOU (Fig. 7e), corresponding to the fact  
 9 that the additional DIC was supplied by organic matter remineralization via aerobic  
 10 respiration. The slope of  $\Delta\text{DIC}$  vs. AOU in the subsurface water was  $0.71 \pm 0.03$ , which  
 11 agrees well with classic Redfield stoichiometry (i.e.,  $106/138=0.77$ ), providing further  
 12 evidence for aerobic respiration as the source of added DIC. As a first order  
 13 comparison, the water column total oxygen consumption rate of  $9.8 \mu\text{mol L}^{-1} \text{d}^{-1}$  could  
 14 well support the oxygen decline rate observed at Station A10 in the hypoxic zone  
 15 between 20 July and 27 July (Fig. 6), which was  $7.7 \mu\text{mol L}^{-1} \text{d}^{-1}$ . This comparison  
 16 along with the stoichiometry between  $\Delta\text{DIC}$  and AOU strongly suggests that water  
 17 column aerobic respiration may be predominate in the formation of the hypoxia in the  
 18 present case.

## 19 4.2 Isotopic composition of the oxygen-consuming OC

20 The DIC isotopic mass balance is shown in Eq. (6) (Wang et al., 2016):

$$21 \delta^{13}\text{C}_{\text{DICobs}} \times \text{DIC}_{\text{obs}} = \delta^{13}\text{C}_{\text{DICcon}} \times \text{DIC}_{\text{con}} + \delta^{13}\text{C}_{\text{DICbio}} \times \text{DIC}_{\text{bio}} \quad (6)$$

22 where the subscripts obs, con and bio refer to the field-observed, conservative and  
 23 biologically altered values.

24 Degradation of OC typically produces DIC with minor isotopic fractionation from  
 25 the OC substrate (Hullar et al., 1996; Breteler et al., 2002). Thus, the isotopic  
 26 composition of  $\text{DIC}_{\text{bio}}$  (i.e.,  $\delta^{13}\text{C}_{\text{DICbio}}$ ) should be identical to the  $\delta^{13}\text{C}$  of the OC  
 27 ( $\delta^{13}\text{C}_{\text{OCx}}$ ), which consumed oxygen and produced  $\text{DIC}_{\text{bio}}$ .  $\delta^{13}\text{C}_{\text{OCx}}$  was derived from the  
 28 mass balance equations of both DIC and its stable isotope:

$$29 \delta^{13}\text{C}_{\text{OCx}} = \frac{\delta^{13}\text{C}_{\text{obs}} \times \text{DIC}_{\text{obs}} - \delta^{13}\text{C}_{\text{con}} \times \text{DIC}_{\text{con}}}{\text{DIC}_{\text{obs}} - \text{DIC}_{\text{con}}} \quad (7)$$

30 Equation (7) can be rearranged into Eq. (8):

$$31 \Delta(\delta^{13}\text{C}_{\text{DIC}} \times \text{DIC}) = \delta^{13}\text{C}_{\text{OCx}} \times \Delta\text{DIC} \quad (8)$$

1 As shown in Fig. 8, the slope of the linear regression represents  $\delta^{13}\text{C}_{\text{OCx}}$  or  $\delta^{13}\text{C}_{\text{DICbio}}$ ,  
2 which here is equal to  $-23.2 \pm 1.1$  ‰. This value reflects the original  $\delta^{13}\text{C}$  signature of  
3 the remineralized organic matter contributing to the observed addition of DIC.

4 Although studies have shown selective diagenesis of isotopically heavy or light pools  
5 of organic matter (Marthur et al., 1992; Lehmann et al., 2002), these effects are small  
6 compared to the isotopic differences among different sources of organic matter  
7 (Meyers, 1997). It is thus reasonable to assume that the isotopic ratios are conservative  
8 and that physical mixing of the end-member sources determine the isotopic  
9 composition of organic matter in natural systems (Gearing et al., 1984; Cifuentes et al.,  
10 1988; Thornton and McManus, 1994). The relative contributions of marine and  
11 terrestrial sources to oxygen-consuming organic matter in our study area could be  
12 estimated based on the following equation (Shultz and Calder, 1976; Hu et al., 2006):

$$13 \quad f(\%) = \frac{\delta^{13}\text{C}_{\text{mar}} - \delta^{13}\text{C}_{\text{OCx}}}{\delta^{13}\text{C}_{\text{mar}} - \delta^{13}\text{C}_{\text{terr}}} \times 100 \quad (9)$$

14 Here, for the terrestrial end-member ( $\delta^{13}\text{C}_{\text{terr}}$ ), we adopted the average  $\delta^{13}\text{C}$  value of  
15 POC sampled near the Humen Outlet ( $S < 4$ ), which represents the predominant source  
16 of riverine material entering the estuary (He et al., 2010b). The mean  $\delta^{13}\text{C}_{\text{POC}}$  value,  
17  $-28.3 \pm 0.7$  ‰ ( $n=7$ ), is very similar to the freshwater  $\delta^{13}\text{C}_{\text{POC}}$  value of  $-28.7$  ‰  
18 reported by Yu et al. (2010), which reflected a terrigenous mixture of C3 plant  
19 fragments and forest soils. For the marine end-member ( $\delta^{13}\text{C}_{\text{mar}}$ ), we calculated the  
20 mean surface water  $\delta^{13}\text{C}_{\text{POC}}$  value ( $-19.4 \pm 0.8$  ‰,  $n=8$ ) from stations with  $S > 26$  where  
21 significant phytoplankton blooms were observed, as indicated by DO supersaturation  
22 ( $\text{DO}\% > 125$  ‰) and relatively high pH values ( $> 8.3$ ) and POC contents ( $5.3 \pm 2.4$  ‰).  
23 This value is similar, although slightly heavier than the marine end-member used by  
24 Chen et al. (2008), who measured a  $\delta^{13}\text{C}$  value of  $-20.9$  ‰ in tow-net phytoplankton  
25 samples from outer Lingdingyang Bay, in the same region as this study. Additionally,  
26 He et al. (2010a) reported a  $\delta^{13}\text{C}$  value of  $-20.8 \pm 0.4$  ‰ in phytoplankton collected  
27 from the northern South China Sea. These values are consistent enough for us to  
28 compile and use an average  $\delta^{13}\text{C}_{\text{mar}}$  value of  $-20.5 \pm 0.9$  ‰. This value agrees well  
29 with the reported stable carbon isotopic signature of marine organic matter in other  
30 coastal regions. For example, mean isotopic values of phytoplankton were reported as  
31  $-20.3 \pm 0.6$  ‰ in Narragansett Bay (Gearing et al., 1984),  $-20.3 \pm 0.9$  ‰ in Auke Bay

1 and Fritz Cove (Goering et al., 1990), and  $-20.1 \pm 0.8$  ‰ in the Gulf of Lions  
2 (Harmelin-Vivien et al., 2008).

3 Our model results suggest that marine organic matter contributed to  $65 \pm 16$  % of the  
4 observed oxygen consumption, while terrestrial organic matter accounted for the  
5 remaining  $35 \pm 16$  %. It is thus clear that marine organic matter from  
6 eutrophication-induced primary production dominated oxygen consumption in the  
7 hypoxic zone; however, terrestrial organic matter also contributed significantly to the  
8 formation and maintenance of hypoxia in the lower PRE and adjacent coastal waters.

### 9 **4.3 Comparison with hypoxia in the East China Sea off the Changjiang Estuary**

10 As one of the largest rivers in the world, the Changjiang has been suffering from  
11 eutrophication for the past few decades (Zhang et al., 1999; Wang et al., 2014). In  
12 summer, sharp density gradients with frequent algal blooms and subsequent organic  
13 matter decomposition cause seasonal hypoxia in the bottom water of the ECS off the  
14 CJE. Wang et al. (2016) revealed that the remineralization of marine organic matter  
15 ( $OC_{\text{mar}}$ ) overwhelmingly (nearly 100 %) contributed to DO consumption in the ECS off  
16 the CJE. However, our present study showed that less  $OC_{\text{mar}}$  contributed to the oxygen  
17 depletion ( $65 \pm 16$  %) in the hypoxic zone of the lower PRE.

18 As shown in Fig. 5, there is little difference between  $\delta^{13}C_{\text{DIC}}$  and  $\delta^{13}C_{\text{POC}}$  values of  
19 the marine end-member. However, the  $\delta^{13}C_{\text{DIC}}$  and  $\delta^{13}C_{\text{POC}}$  values of the freshwater  
20 end-member showed some dissimilarity, with lighter values in the PRE ( $-11.4 \pm 0.2$  ‰,  
21  $-28.3 \pm 0.7$  ‰) than in the CJE ( $-8.8$  ‰,  $-24.4 \pm 0.2$  ‰). In Fig. 7e, the amplitude of  
22  $\Delta\text{DIC}$  and AOU values suggest a similar intensity of OM biodegradation, and the  
23 slope of  $\Delta\text{DIC}$  vs. AOU ( $0.71 \pm 0.03$  vs.  $0.65 \pm 0.04$ ) indicates a predominance of  
24 aerobic respiration in the two systems. As seen from Table 2, there is no significant  
25 difference between the  $\delta^{13}C$  values of surface sediments within the hypoxic zones of  
26 the PRE and CJE. However, data in Fig. 7a show generally higher water temperatures  
27 in the PRE than in the CJE. For instance, the temperature of surface and subsurface  
28 seawater end-members in the PRE is 2-3 °C higher than in the CJE. From a spatial  
29 point of view, the distance from the river mouth to the hypoxic zone in the CJE is 2-3  
30 times longer than in the PRE, possibly resulting in a longer travel time of  $OC_{\text{terr}}$ .  
31 Therefore, we contend that the difference in the predicted distributions of marine and  
32 terrestrial sources of organic matter contributing to oxygen consumption in and off the

1 PRE and CJE is likely related to differences in the bioavailability of  $OC_{terr}$  and  $OC_{mar}$ ,  
2 the microbial community structures and the physical settings between these two  
3 hypoxic systems.

4 Although C3 plants dominate and C4 plants are minor in both the Pearl River and  
5 Changjiang drainage basins (Hu et al., 2006; Zhu et al., 2011a), the  $OC_{terr}$  delivered  
6 from these two watersheds experiences varying degrees of degradation within the  
7 estuaries before being transported into the coastal hypoxic zones. In the CJE,  
8 approximately 50 % of  $OC_{terr}$  becomes remineralized during transport through the  
9 estuary, likely due to efficient OM unloading from mineral surfaces (Zhu et al., 2011a)  
10 and longer residence times within the estuary, facilitating microbial transformation and  
11 degradation. In contrast, the PRE appears to be a somewhat intermediate site with the  
12 export of  $OC_{terr}$  being closely associated with sedimentary regimes and not  
13 characterized by extensive degradative loss (Strong et al., 2012). Thus, the  
14 bioavailability of  $OC_{terr}$  that reached the hypoxic zone is likely higher in the PRE than  
15 in the CJE. Moreover, the increased precipitation and runoff during the typhoon may  
16 have mobilized additional fresh anthropogenic OM from surrounding megacities (e.g.  
17 Guangzhou, Shenzhen and Zhuhai) deposited in the river channel, which could lead to  
18 more labile  $OC_{terr}$  in the PRE. Additionally, the difference in bacterial community  
19 structure between the two systems may have played a role. Recent studies have  
20 demonstrated that the bacterial community in the PRE is characterized by higher  
21 relative abundances of Actinobacteria and lower relative abundances of  
22 Cytophaga-Flavobacteria-Bacteroides (CFB) than in the CJE (Liu et al., 2012; Zhang et  
23 al., 2016). Whether such differences would promote the degradation of  $OC_{terr}$  in the  
24 PRE relative to the CJE remains unknown. Finally, the temperature of the bottom water  
25 in the PRE hypoxic zone (27–29 °C) was higher than in the CJE hypoxic zone (21.5–  
26 24.0 °C), which may have accelerated the rates of bacterial growth and OM  
27 decomposition (Brown et al., 2004).

## 28 **5 Conclusions**

29 Based on a three end-member mixing model and the mass balance of DIC and its  
30 isotopic composition, we demonstrated that the organic matter decomposed via aerobic  
31 respiration in the stratified subsurface waters of the lower PRE and adjacent coastal  
32 waters was predominantly  $OC_{mar}$  (49-81 %, mean 65 %), with a significant portion of

1 OC<sub>terr</sub> also decomposed (19-51 %, mean 35 %). The relative distribution of organic  
2 matter sources contributing to oxygen drawdown differs in the hypoxic zone off the  
3 CJE, where it is caused almost entirely by OC<sub>mar</sub>. These differences have important  
4 implications for better understanding the controls on hypoxia and its mitigation.  
5 Nevertheless, with respect to increasing coastal nutrient levels, a significant implication  
6 of the present study is that reducing and managing nutrients is critical to control  
7 eutrophication and, subsequently, to mitigate hypoxia (Conley et al., 2009; Paerl, 2009;  
8 Mercedes et al., 2015; Stefan et al., 2016). Given that OC<sub>terr</sub> also contributes to the  
9 consumption of oxygen in the lower PRE hypoxic zone, it is crucial to characterize the  
10 source of this oxygen-consuming terrestrial organic matter, whether from natural soil  
11 leaching and/or anthropogenic wastewater discharge, so as to make proper policies for  
12 hypoxia remediation.

13 The processes involved in the partitioning of organic matter sources, their isotopic  
14 signals and their subsequent biogeochemical transformations in the PRE hypoxic zone  
15 are illustrated in the conceptual diagram in Fig. 9. The river delivers a significant  
16 amount of nutrients and terrestrial organic matter to the estuary, stimulating  
17 phytoplankton blooms in the surface water at the lower reaches of the estuary where  
18 turbidity is relatively low and conditions are favourable for phytoplankton growth  
19 (Gaston et al., 2006; Dai et al., 2008b; Guo et al., 2009). The subsequent sinking of this  
20 biomass along with terrestrial organic matter below the pycnocline consumes oxygen  
21 and adds respired DIC to subsurface waters, resulting in coastal hypoxia. Therefore, we  
22 conclude that within the PRE and adjacent coastal areas, the most important biological  
23 process with respect to forming and maintaining hypoxic conditions is aerobic  
24 respiration.

25  
26  
27

28 *Acknowledgments.* This research was funded by the National Natural Science  
29 Foundation of China through grants 41130857, 41576085 and 41361164001. We thank  
30 Tengxiang Xie, Li Ma, Shengyao Sun, Chenhe Zheng and Liangrong Zou for their  
31 assistance in sample collections; Yan Li and Yawen Wei for providing the calcium  
32 concentration data; Liguó Guo, Tao Huang and Dawei Li for assisting on the  
33 measurements of DIC, nutrients and  $\delta^{13}\text{C}_{\text{POC}}$ . The captain and the crew of R/V *Kediao 8*

1 are acknowledged for their cooperation during the cruise. Finally, we express our  
2 gratitude to three anonymous referees for their insightful and constructive comments  
3 and input.

## 7 **References**

8 Bianchi, T. S.: The role of terrestrially derived organic carbon in the coastal ocean: A  
9 changing paradigm and the priming effect, *Proc. Natl. Acad. Sci. U.S.A.*, 108,  
10 19473-19481, doi:10.1073/pnas.1017982108, 2011a.

11 Bianchi, T. S., Wysocki, L. A., Schreiner, K. M., Filley, T. R., Corbett, D. R., and  
12 Kolker, A. S.: Sources of terrestrial organic carbon in the Mississippi plume region:  
13 evidence for the importance of coastal marsh inputs, *Aquat. Geochem.*, 17, 431-456,  
14 doi:10.1007/s10498-010-9110-3, 2011b.

15 Boesch, D. F., Boynton, W. R., Crowder, L. B., Diaz, R. J., Howarth, R. W., Mee, L. D.,  
16 Nixon, S. W., Rabalais, N. N., Rosenberg, R., Sanders, J. G., Scavia, D., and Turner,  
17 R. E.: Nutrient Enrichment Drives Gulf of Mexico Hypoxia, *Eos, Trans. Amer.*  
18 *Geophys. Union*, 90, 117-118, doi:10.1029/2009EO140001, 2009.

19 Breitburg, D.: Effects of hypoxia, and the balance between hypoxia and enrichment, on  
20 coastal fishes and fisheries, *Estuaries*, 25, 767-781, doi:10.1007/BF02804904, 2002.

21 Breteler, W. C. K., Grice, K., Schouten, S., Kloosterhuis, H. T., and Damsté J. S. S.:  
22 Stable carbon isotope fractionation in the marine copepod *Temora longicornis*:  
23 unexpectedly low  $\delta^{13}\text{C}$  value of faecal pellets, *Mar. Ecol. Prog. Ser.*, 240, 195-204,  
24 doi:10.3354/meps240195, 2002.

25 Brown, J. H., Gillooly, J. F., Allen, A. P., Savage, V. M., and West, G. B.: Toward a  
26 metabolic theory of ecology, *Ecology*, 85, 1771-1789, doi:10.1890/03-9000, 2004.

27 Cai, W.-J., Dai, M., Wang, Y., Zhai, W., Huang, T., Chen, S., Zhang, F., Chen, Z., and  
28 Wang, Z.: The biogeochemistry of inorganic carbon and nutrients in the Pearl River  
29 estuary and the adjacent Northern South China Sea, *Cont. Shelf Res.*, 24, 1301-1319,  
30 doi:10.1016/j.csr.2004.04.005, 2004.

31 Cao, Z., Dai, M., Zheng, N., Wang, D., Li, Q., Zhai, W., Meng, F., and Gan, J.:  
32 Dynamics of the carbonate system in a large continental shelf system under the

1 influence of both a river plume and coastal upwelling, *J. Geophys. Res. Biogeosci.*,  
2 116, G02010, doi:10.1029/2010JG001596, 2011.

3 Carstensen, J., Andersen, J. H., Gustafsson, B. G., and Conley, D. J.: Deoxygenation of  
4 the Baltic Sea during the last century, *Proc. Natl. Acad. Sci. U.S.A.*, 111, 5628-5633,  
5 doi:10.1073/pnas.1323156111, 2014.

6 Chen, F., Zhang, L., Yang, Y., and Zhang, D.: Chemical and isotopic alteration of  
7 organic matter during early diagenesis: Evidence from the coastal area off-shore the  
8 Pearl River estuary, south China, *J. Mar. Syst.*, 74, 372-380,  
9 doi:10.1016/j.jmarsys.2008.02.004, 2008.

10 Cifuentes, L., Sharp, J., and Fogel, M. L.: Stable carbon and nitrogen isotope  
11 biogeochemistry in the Delaware estuary, *Limnol. Oceanogr.*, 33, 1102-1115,  
12 doi:10.4319/lo.1988.33.5.1102, 1988.

13 Conley, D. J., Paerl, H. W., Howarth, R. W., Boesch, D. F., Seitzinger, S. P., Karl, E.,  
14 Karl, E., Lancelot, C., Gene, E., and Gene, E.: Controlling eutrophication: nitrogen  
15 and phosphorus, *Science*, 123, 1014-1015, doi:10.1126/science.1167755, 2009.

16 Dai, M., Guo, X., Zhai, W., Yuan, L., Wang, B., Wang, L., Cai, P., Tang, T., and Cai,  
17 W.-J.: Oxygen depletion in the upper reach of the Pearl River estuary during a winter  
18 drought, *Mar. Chem.*, 102, 159-169, doi:10.1016/j.marchem.2005.09.020, 2006.

19 Dai, M., Wang, L., Guo, X., Zhai, W., Li, Q., He, B., and Kao, S.-J.: Nitrification and  
20 inorganic nitrogen distribution in a large perturbed river/estuarine system: the Pearl  
21 River Estuary, China, *Biogeosciences*, 5, 1227-1244, doi:10.5194/bg-5-1227-2008,  
22 2008a.

23 Dai, M., Zhai, W., Cai, W.-J., Callahan, J., Huang, B., Shang, S., Huang, T., Li, X., Lu,  
24 Z., Chen, W., and Chen, Z.: Effects of an estuarine plume-associated bloom on the  
25 carbonate system in the lower reaches of the Pearl River estuary and the coastal zone  
26 of the northern South China Sea, *Cont. Shelf Res.*, 28, 1416-1423, doi:  
27 10.1016/j.csr.2007.04.018, 2008b.

28 Diaz, R. J. and Rosenberg, R.: Spreading dead zones and consequences for marine  
29 ecosystems, *Science*, 321, 926-929, doi:10.1126/science.1156401, 2008.

30 Gaston, T. F., Schlacher, T. A., and Connolly, R. M.: Flood discharges of a small river  
31 into open coastal waters: Plume traits and material fate, *Estuar. Coast. Shelf Sci.*, 69,  
32 4-9, doi:10.1016/j.ecss.2006.03.015, 2006.



- 1 Gearing, J. N., Gearing, P. J., Rudnick, D. T., Requejo, A. G., and Hutchins, M. J.:  
2 Isotopic variability of organic carbon in a phytoplankton-based, temperate estuary,  
3 *Geochim. Cosmochim. Acta*, 48, 1089-1098, doi:10.1016/0016-7037(84)90199-6,  
4 1984.
- 5 Goering, J., Alexander, V., and Haubenstock, N.: Seasonal variability of stable carbon  
6 and nitrogen isotope ratios of organisms in a North Pacific Bay, *Estuar. Coast. Shelf*  
7 *Sci.*, 30, 239-260, doi:10.1016/0272-7714(90)90050-2, 1990.
- 8 Guo, X., Dai, M., Zhai, W., Cai, W.-J., and Chen, B.: CO<sup>2</sup> flux and seasonal variability  
9 in a large subtropical estuarine system, the Pearl River Estuary, China, *J. Geophys.*  
10 *Res. Biogeosci.*, 114, G03013, doi:10.1029/2008JG000905, 2009.
- 11 Guo, X. and Wong, G. T.: Carbonate chemistry in the northern South China Sea  
12 shelf-sea in June 2010, *Deep-Sea Res. II*, 117, 119-130,  
13 doi:10.1016/j.dsr2.2015.02.024, 2015.
- 14 Han, A., Dai, M., Kao, S.-J., Gan, J., Li, Q., Wang, L., Zhai, W., and Wang, L.: Nutrient  
15 dynamics and biological consumption in a large continental shelf system under the  
16 influence of both a river plume and coastal upwelling, *Limnol. Oceanogr.*, 57,  
17 486-502, doi:10.4319/lo.2012.57.2.0486, 2012.
- 18 Harmelin-Vivien, M., Loizeau, V., Mellon, C., Beker, B., Arlhac, D., Bodiguel, X.,  
19 Ferraton, F., Hermand, R., Philippon, X., and Salen-Picard, C.: Comparison of C and  
20 N stable isotope ratios between surface particulate organic matter and  
21 microphytoplankton in the Gulf of Lions (NW Mediterranean), *Cont. Shelf Res.*, 28,  
22 1911-1919, 2008.
- 23 He, B., Dai, M., Huang, W., Liu, Q., Chen, H., and Xu, L.: Sources and accumulation of  
24 organic carbon in the Pearl River Estuary surface sediment as indicated by elemental,  
25 stable carbon isotopic, and carbohydrate compositions, *Biogeosciences*, 7,  
26 3343-3362, doi:10.5194/bg-7-3343-2010, 2010a.
- 27 He, B., Dai, M., Zhai, W., Wang, L., Wang, K., Chen, J., Lin, J., Han, A., and Xu, Y.:  
28 Distribution, degradation and dynamics of dissolved organic carbon and its major  
29 compound classes in the Pearl River estuary, China, *Mar. Chem.*, 119, 52-64,  
30 doi:10.1016/j.marchem.2009.12.006, 2010b.
- 31 He, B., Dai, M., Zhai, W., Guo, X., and Wang, L.: Hypoxia in the upper reaches of the  
32 Pearl River Estuary and its maintenance mechanisms: A synthesis based on multiple

1 year observations during 2000–2008, *Mar. Chem.*, 167, 13-24,  
2 doi:10.1016/j.marchem.2014.07.003, 2014.

3 He, G.-f. and Yuan, G.-m.: Assessment of the water quality by fuzzy mathematics for  
4 last 20 years in Zhujiang Estuary, *Mar. Environ. Sci.*, 26, 53-57, 2007.

5 Hu, J., Peng, P. a., Jia, G., Mai, B., and Zhang, G.: Distribution and sources of organic  
6 carbon, nitrogen and their isotopes in sediments of the subtropical Pearl River estuary  
7 and adjacent shelf, Southern China, *Mar. Chem.*, 98, 274-285,  
8 doi:10.1016/j.marchem.2005.03.008, 2006.

9 Huang, X., Huang, L., and Yue, W.: The characteristics of nutrients and eutrophication  
10 in the Pearl River estuary, South China, *Mar. Pollut. Bull.*, 47, 30-36,  
11 doi:10.1016/S0025-326X(02)00474-5, 2003.

12 Hullar, M., Fry, B., Peterson, B., and Wright, R.: Microbial utilization of estuarine  
13 dissolved organic carbon: a stable isotope tracer approach tested by mass balance,  
14 *Appl. Environ. Microbiol.*, 62, 2489-2493, 1996.

15 Kao, S.-J., Terence Yang, J.-Y., Liu, K.-K., Dai, M., Chou, W.-C., Lin, H.-L., and Ren,  
16 H.: Isotope constraints on particulate nitrogen source and dynamics in the upper water  
17 column of the oligotrophic South China Sea, *Global Biogeochem. Cycles*, 26,  
18 GB2033, doi:10.1029/2011GB004091, 2012.

19 Kao, S. J., Lin, F. J., and Liu, K. K.: Organic carbon and nitrogen contents and their  
20 isotopic compositions in surficial sediments from the East China Sea shelf and the  
21 southern Okinawa Trough, *Deep Sea Res. Part II: Top. Stud. Oceanogr.*, 50,  
22 1203-1217, doi:10.1016/S0967-0645(03)00018-3, 2003.

23 Kemp, W., Testa, J., Conley, D., Gilbert, D., and Hagy, J.: Temporal responses of  
24 coastal hypoxia to nutrient loading and physical controls, *Biogeosciences*, 6,  
25 2985-3008, doi:10.5194/bg-6-2985-2009, 2009.

26 Lehmann, M. F., Bernasconi, S. M., Barbieri, A., and McKenzie, J. A.: Preservation of  
27 organic matter and alteration of its carbon and nitrogen isotope composition during  
28 simulated and in situ early sedimentary diagenesis, *Geochim. Cosmochim. Acta*, 66,  
29 3573-3584, doi:10.1016/S0016-7037(02)00968-7, 2002.

30 Li, D., Zhang, J., Huang, D., Wu, Y., and Liang, J.: Oxygen depletion off the  
31 Changjiang (Yangtze River) estuary, *Sci. China Ser. D-Earth Sci.*, 45, 1137-1146,  
32 doi:10.1360/02yd9110, 2002.

- 1 Liu, M., Xiao, T., Wu, Y., Zhou, F., Huang, H., Bao, S., and Zhang, W.: Temporal  
2 distribution of bacterial community structure in the Changjiang Estuary hypoxia area  
3 and the adjacent East China Sea, *Environ. Res. Lett.*, 7, 025001,  
4 doi:10.1088/1748-9326/7/2/025001, 2012.
- 5 Marthur, J. M., Tyson, R. V., Thomson, J., and Matthey, D.: Early diagenesis of marine  
6 organic matter: Alteration of the carbon isotopic composition, *Mar. Geol.*, 105,  
7 51-61, doi:10.1016/0025-3227(92)90181-G, 1992.
- 8 Mercedes, M. C. B., Luiz Antonio, M., Tibisay, P., Rafael, R., Jean Pierre, H. B. O.,  
9 Felipe Siqueira, P., Silvia Rafaela Machado, L., and Sorena, M.: Nitrogen  
10 management challenges in major watersheds of South America, *Environ. Res. Lett.*,  
11 10, 065007, doi:10.1088/1748-9326/10/6/065007, 2015.
- 12 Meyers, P. A.: Organic geochemical proxies of paleoceanographic, paleolimnologic,  
13 and paleoclimatic processes, *Org. Geochem.*, 27, 213-250,  
14 doi:10.1016/S0146-6380(97)00049-1, 1997.
- 15 Nixon, S. W.: Coastal marine eutrophication: A definition, social causes, and future  
16 concerns, *Ophelia*, 41, 199-219, doi:10.1080/00785236.1995.10422044, 1995.
- 17 Paerl, H. W.: Assessing and managing nutrient-enhanced eutrophication in estuarine  
18 and coastal waters: Interactive effects of human and climatic perturbations, *Ecol.*  
19 *Eng.*, 26, 40-54, doi:10.1016/j.ecoleng.2005.09.006, 2006.
- 20 Paerl, H. W.: Controlling Eutrophication along the Freshwater–Marine Continuum:  
21 Dual Nutrient (N and P) Reductions are Essential, *Estuar. Coast.*, 32, 593-601,  
22 doi:10.1007/s12237-009-9158-8, 2009.
- 23 Peterson, B. J. and Fry, B.: Stable Isotopes in Ecosystem Studies, *Annu. Rev. Ecol.*  
24 *Syst.*, 18, 293-320, 1987.
- 25 Qian, W., Dai, M., Xu, M., Kao, S.-j., Du, C., Liu, J., Wang, H., Guo, L., and Wang, L.:  
26 Non-local drivers of the summer hypoxia in the East China Sea off the Changjiang  
27 Estuary, *Estuar. Coast. Shelf Sci.*, doi:10.1016/j.ecss.2016.08.032, 2016.
- 28 Qian, W., Gan, J., Liu, J., He, B., Lu, Z., Guo, X., Wang, D., Guo, L., Huang, T., and  
29 Dai, M.: Current status of emerging hypoxia in a large eutrophic estuary: the lower  
30 reach of Pearl River estuary, China, Submitted to *Limnol. Oceanogr.*, 2017.
- 31 Rabalais, N., Cai, W.-J., Carstensen, J., Conley, D., Fry, B., Hu, X., Qui ñones-Rivera,  
32 Z., Rosenberg, R., Slomp, C., Turner, E., Voss, M., Wissel, B., and Zhang, J.:

1 Eutrophication-Driven Deoxygenation in the Coastal Ocean, *Oceanography*, 27,  
2 172-183, doi:10.5670/oceanog.2014.21, 2014.

3 Rabalais, N. N., D'áz, R. J., Levin, L. A., Turner, R. E., Gilbert, D., and Zhang, J.:  
4 Dynamics and distribution of natural and human-caused hypoxia, *Biogeosciences*, 7,  
5 585-619, doi:10.5194/bg-7-585-2010, 2010.

6 Rabouille, C., Conley, D. J., Dai, M. H., Cai, W. J., Chen, C. T. A., Lansard, B., Green,  
7 R., Yin, K., Harrison, P. J., Dagg, M., and McKee, B.: Comparison of hypoxia among  
8 four river-dominated ocean margins: The Changjiang (Yangtze), Mississippi, Pearl,  
9 and Rhône rivers, *Cont. Shelf Res.*, 28, 1527-1537, doi:10.1016/j.csr.2008.01.020,  
10 2008.

11 Rutger, R., Stefan, A., Birthe, H., Hans, C. N., and Karl, N.: Recovery of marine  
12 benthic habitats and fauna in a Swedish fjord following improved oxygen conditions,  
13 *Mar. Ecol. Prog. Ser.*, 234, 43-53, doi:10.3354/meps234043, 2002.

14 Shultz, D. J. and Calder, J. A.: Organic carbon  $^{13}\text{C}/^{12}\text{C}$  variations in estuarine  
15 sediments, *Geochim. Cosmochim. Acta*, 40, 381-385,  
16 doi:10.1016/0016-7037(76)90002-8, 1976.

17 Steckbauer, A., Duarte, C. M., Carstensen, J., Vaquer-Sunyer, R., and Conley, D. J.:  
18 Ecosystem impacts of hypoxia: thresholds of hypoxia and pathways to recovery,  
19 *Environ. Res. Lett.*, 6, 025003, doi:10.1088/1748-9326/6/2/025003, 2011.

20 Stefan, R., Mateete, B., Clare, M. H., Nancy, K., Wilfried, W., Xiaoyuan, Y., Albert,  
21 B., and Mark, A. S.: Synthesis and review: Tackling the nitrogen management  
22 challenge: from global to local scales, *Environ. Res. Lett.*, 11, 120205,  
23 doi:10.1088/1748-9326/11/12/120205, 2016.

24 Strong, D. J., Flecker, R., Valdes, P. J., Wilkinson, I. P., Rees, J. G., Zong, Y. Q., Lloyd,  
25 J. M., Garrett, E., and Pancost, R. D.: Organic matter distribution in the modern  
26 sediments of the Pearl River Estuary, *Org. Geochem.*, 49, 68-82,  
27 doi:10.1016/j.orggeochem.2012.04.011, 2012.

28 Swarzenski, P., Campbell, P., Osterman, L., and Poore, R.: A 1000-year sediment  
29 record of recurring hypoxia off the Mississippi River: The potential role of  
30 terrestrially-derived organic matter inputs, *Mar. Chem.*, 109, 130-142,  
31 doi:10.1016/j.marchem.2008.01.003, 2008.

1 Tan, F. C., Cai, D. L., and Edmond, J. M.: Carbon isotope geochemistry of the  
2 Changjiang estuary, *Estuar. Coast. Shelf Sci.*, 32, 395-403,  
3 doi:10.1016/0272-7714(91)90051-C, 1991.

4 Thornton, S. F. and McManus, J.: Application of Organic Carbon and Nitrogen Stable  
5 Isotope and C/N Ratios as Source Indicators of Organic Matter Provenance in  
6 Estuarine Systems: Evidence from the Tay Estuary, Scotland, *Estuar. Coast. Shelf  
7 Sci.*, 38, 219-233, doi:10.1006/ecss.1994.1015, 1994.

8 Vaquer-Sunyer, R. and Duarte, C. M.: Thresholds of hypoxia for marine biodiversity,  
9 *Proc. Natl. Acad. Sci. U.S.A.*, 105, 15452-15457, doi:10.1073/pnas.0803833105,  
10 2008.

11 Wang, H., Dai, M., Liu, J., Kao, S.-J., Zhang, C., Cai, W.-J., Wang, G., Qian, W., Zhao,  
12 M., and Sun, Z.: Eutrophication-Driven Hypoxia in the East China Sea off the  
13 Changjiang Estuary, *Environ. Sci. Technol.*, 50, 2255-2263,  
14 doi:10.1021/acs.est.5b06211, 2016.

15 Wang, Q., Koshikawa, H., Liu, C., and Otsubo, K.: 30-year changes in the nitrogen  
16 inputs to the Yangtze River Basin, *Environ. Res. Lett.*, 9, 115005,  
17 doi:10.1088/1748-9326/9/11/115005, 2014.

18 Xing, L., Zhang, H., Yuan, Z., Sun, Y., and Zhao, M.: Terrestrial and marine biomarker  
19 estimates of organic matter sources and distributions in surface sediments from the  
20 East China Sea shelf, *Cont. Shelf Res.*, 31, 1106-1115,  
21 doi:10.1016/j.csr.2011.04.003, 2011.

22 Yao, P., Zhao, B., Bianchi, T. S., Guo, Z., Zhao, M., Li, D., Pan, H., Wang, J., Zhang,  
23 T., and Yu, Z.: Remineralization of sedimentary organic carbon in mud deposits of  
24 the Changjiang Estuary and adjacent shelf: Implications for carbon preservation and  
25 authigenic mineral formation, *Cont. Shelf Res.*, 91, 1-11,  
26 doi:10.1016/j.csr.2014.08.010, 2014.

27 Ye, F., Huang, X., Zhang, X., Zhang, D., Zeng, Y., and Tian, L.: Recent oxygen  
28 depletion in the Pearl River Estuary, South China: geochemical and microfaunal  
29 evidence, *J. Oceanogr.*, 68, 387-400, doi:10.1007/s10872-012-0104-1, 2012.

30 Yu, F., Zong, Y., Lloyd, J. M., Huang, G., Leng, M. J., Kendrick, C., Lamb, A. L., and  
31 Yim, W. W.-S.: Bulk organic  $\delta^{13}\text{C}$  and C/N as indicators for sediment sources in the  
32 Pearl River delta and estuary, southern China, *Estuar. Coast. Shelf Sci.*, 87, 618-630,  
33 doi:10.1016/j.ecss.2010.02.018, 2010.

1 Zhang, J., Zhang, Z. F., Liu, S. M., Wu, Y., Xiong, H., and Chen, H. T.: Human impacts  
2 on the large world rivers: Would the Changjiang (Yangtze River) be an illustration?,  
3 *Global Biogeochem. Cycles*, 13, 1099-1105, doi:10.1029/1999GB900044, 1999.

4 Zhang, J., Cowie, G., and Naqvi, S. W. A.: Hypoxia in the changing marine  
5 environment, *Environ. Res. Lett.*, 8, 015025, doi:10.1088/1748-9326/8/1/015025,  
6 2013.

7 Zhang, Y., Xiao, W., and Jiao, N.: Linking biochemical properties of particles to  
8 particle-attached and free-living bacterial community structure along the particle  
9 density gradient from freshwater to open ocean, *J. Geophys. Res. Biogeosci.*, 121,  
10 2261-2274, doi:10.1002/2016JG003390, 2016.

11 Zhao, H.-D., Kao, S.-J., Zhai, W.-D., Zang, K.-P., Zheng, N., Xu, X.-M., Huo, C., and  
12 Wang, J.-Y.: Effects of stratification, organic matter remineralization and bathymetry  
13 on summertime oxygen distribution in the Bohai Sea, China, *Cont. Shelf Res.*, 134,  
14 15-25, doi:10.1016/j.csr.2016.12.004, 2017.

15 Zhu, C., Wagner, T., Pan, J.-M., and Pancost, R. D.: Multiple sources and extensive  
16 degradation of terrestrial sedimentary organic matter across an energetic, wide  
17 continental shelf, *Geochem. Geophys. Geosyst.*, 12, Q08011,  
18 doi:10.1029/2011GC003506, 2011a.

19 Zhu, Z.-Y., Zhang, J., Wu, Y., Zhang, Y.-Y., Lin, J., and Liu, S.-M.: Hypoxia off the  
20 Changjiang (Yangtze River) Estuary: oxygen depletion and organic matter  
21 decomposition, *Mar. Chem.*, 125, 108-116, doi:10.1016/j.marchem.2011.03.005,  
22 2011b.

23 Zimmerman, A. R. and Canuel, E. A.: A geochemical record of eutrophication and  
24 anoxia in Chesapeake Bay sediments: anthropogenic influence on organic matter  
25 composition, *Mar. Chem.*, 69, 117-137, doi:10.1016/S0304-4203(99)00100-0, 2000.

26 Zong, Y., Lloyd, J., Leng, M., Yim, W.-S., and Huang, G.: Reconstruction of Holocene  
27 monsoon history from the Pearl River Estuary, southern China, using diatoms and  
28 carbon isotope ratios, *Holocene*, 16, 251-263, doi:10.1191/0959683606hl911rp,  
29 2006.

30  
31  
32  
33

1 **Table 1.** Summary of end-member values and their uncertainties adopted in the three  
 2 end-member mixing model.

| Water<br>Mass | $\theta(^{\circ}\text{C})$ | Salinity       | DIC<br>( $\mu\text{mol kg}^{-1}$ ) | $\delta^{13}\text{C}_{\text{DIC}}$<br>(‰) | $\text{Ca}^{2+}$<br>( $\mu\text{mol kg}^{-1}$ ) |
|---------------|----------------------------|----------------|------------------------------------|---|---|
| Plume         | $30.6 \pm 1.0$             | 10.8           | $1670 \pm 50^{\text{a}}$           | $-7.0 \pm 0.8^{\text{b}}$                 | $3670 \pm 16^{\text{c}}$                        |
| Surface       | $31.0 \pm 1.0$             | $33.7 \pm 0.2$ | $1917 \pm 3$                       | $0.6 \pm 0.2$                             | $9776 \pm 132^{\text{c}}$                       |
| Subsurface    | $21.8 \pm 1.0$             | $34.6 \pm 0.1$ | $2023 \pm 6$                       | $0.1 \pm 0.1$                             | 10053   |

3 <sup>a</sup> In order to derive a proper plume end-member value, we took advantage of 3 years of surface  
 4 dataset from summer cruises (see Sect. 4.1). For DIC, the data is from cruises during August  
 5 2012, July 2014 and July 2015.

6 <sup>b</sup> See details in Sect. 4.1.

7 <sup>c</sup> The  $\text{Ca}^{2+}$  values of the plume and surface seawater end-member are derived from a  
 8 conservative mixing calculation ( $\text{Ca}^{2+}$  vs. S) based on 3 years of surface data during the summer  
 9 (August 2012, July 2014 and July 2015).

10  
 11  
 12  
 13  
 14  
 15  
 16  
 17  
 18  
 19  
 20  
 21  
 22  
 23  
 24  
 25  
 26  
 27  
 28  
 29  
 30

1 **Table 2.** Comparison of  $\delta^{13}\text{C}$  values in surface sediments within the hypoxic zone<sup>a</sup> between  
 2 the PRE and CJE.

| $\delta^{13}\text{C}$ (‰)  | Mean $\pm$ SD   | Stations involved                  | References       |
|----------------------------|-----------------|------------------------------------|------------------|
| <u>Pearl River Estuary</u> |                 |                                    |                  |
| -23.4 ~ -22.1              | -22.9 $\pm$ 0.5 | A4, A5, C1-C4, D1                  | Hu et al. 2006   |
| -23.2 ~ -22.3              | -22.7 $\pm$ 0.5 | 28, 29, 30                         | Zong et al. 2006 |
| -23.6 ~ -21.5              | -22.5 $\pm$ 1.1 | E8-1, E7A, S7-1, S7-2              | He et al. 2010a  |
| - <sup>b</sup>             | -23.1 $\pm$ 0.6 | Clustering groups G6 and G7        | Yu et al. 2010   |
| Average                    | -22.8 $\pm$ 0.6 |                                    |                  |
| <u>Changjiang Estuary</u>  |                 |                                    |                  |
| -22.9 ~ -20.9              | -21.8 $\pm$ 0.6 | - <sup>c</sup>                     | Tan et al. 1991  |
| -22.4 ~ -19.9              | -21.2 $\pm$ 1.0 | 32, 37, 38, 42, 48, 49, 54, 56, 64 | Kao et al. 2003  |
| -22.7 ~ -20.8              | -22.0 $\pm$ 0.8 | H1-12, H2-10, H2-11, S1-2, S2-4    | Xing et al. 2011 |
| -23.5 ~ -20.4              | -22.6 $\pm$ 1.0 | 3, 12, 13, 20-25                   | Yao et al. 2014  |
| Average                    | -21.9 $\pm$ 1.0 |                                    |                  |

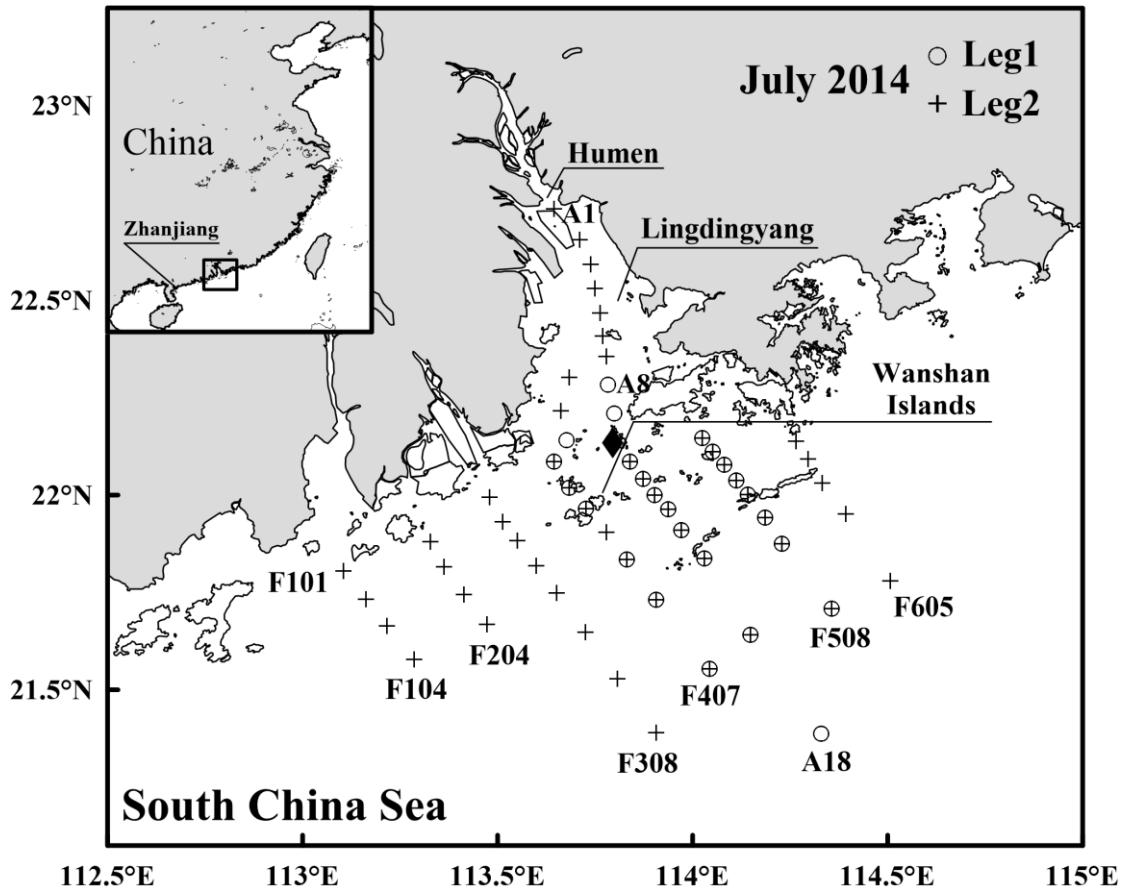
3 <sup>a</sup>In the PRE, the data is from similar sites to our present study, which is in the northeast (Leg 1)  
 4 and southwest (Leg 2) of the Wanshan Islands. While in the CJE, the hypoxic zone is located  
 5 around 30.0 °N–32.0 °N, 122.7 °E–123.2 °E, which is frequently reported in previous studies  
 6 (Li et al., 2002; Zhu et al., 2011b; Wang et al., 2016).

7 <sup>b</sup>The authors provide an average value of clustering groups instead of individual data from each  
 8 site.

9 <sup>c</sup>In Fig. 7 of Tan et al. (1991), the sampling sites are shown without numbers.

10  
 11  
 12  
 13  
 14  
 15  
 16  
 17  
 18  
 19





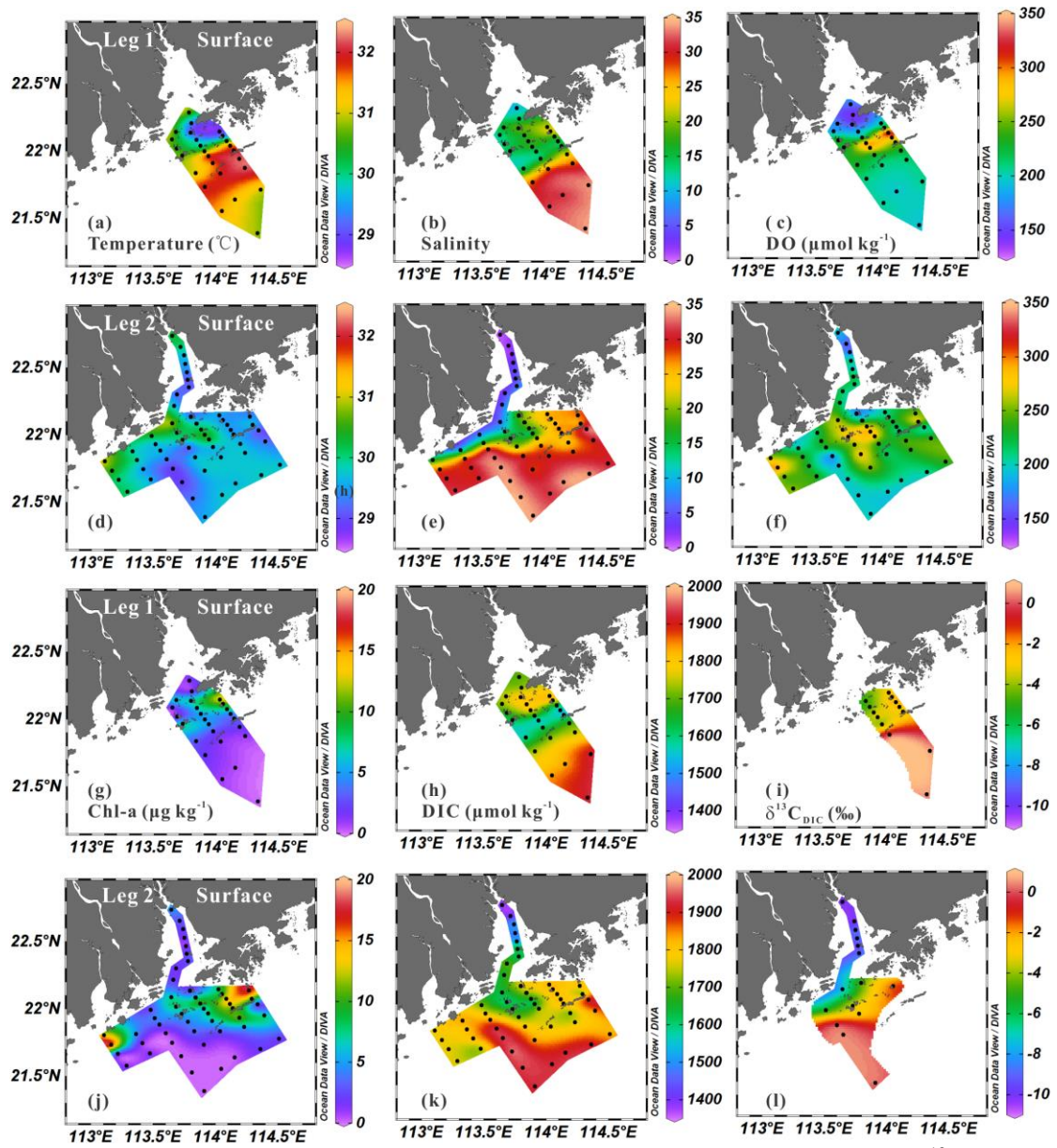
1            112.5°E            113°E            113.5°E            114°E            114.5°E            115°E

2    **Figure 1.** Map of the Pearl River Estuary and adjacent coastal waters. The open circles denote

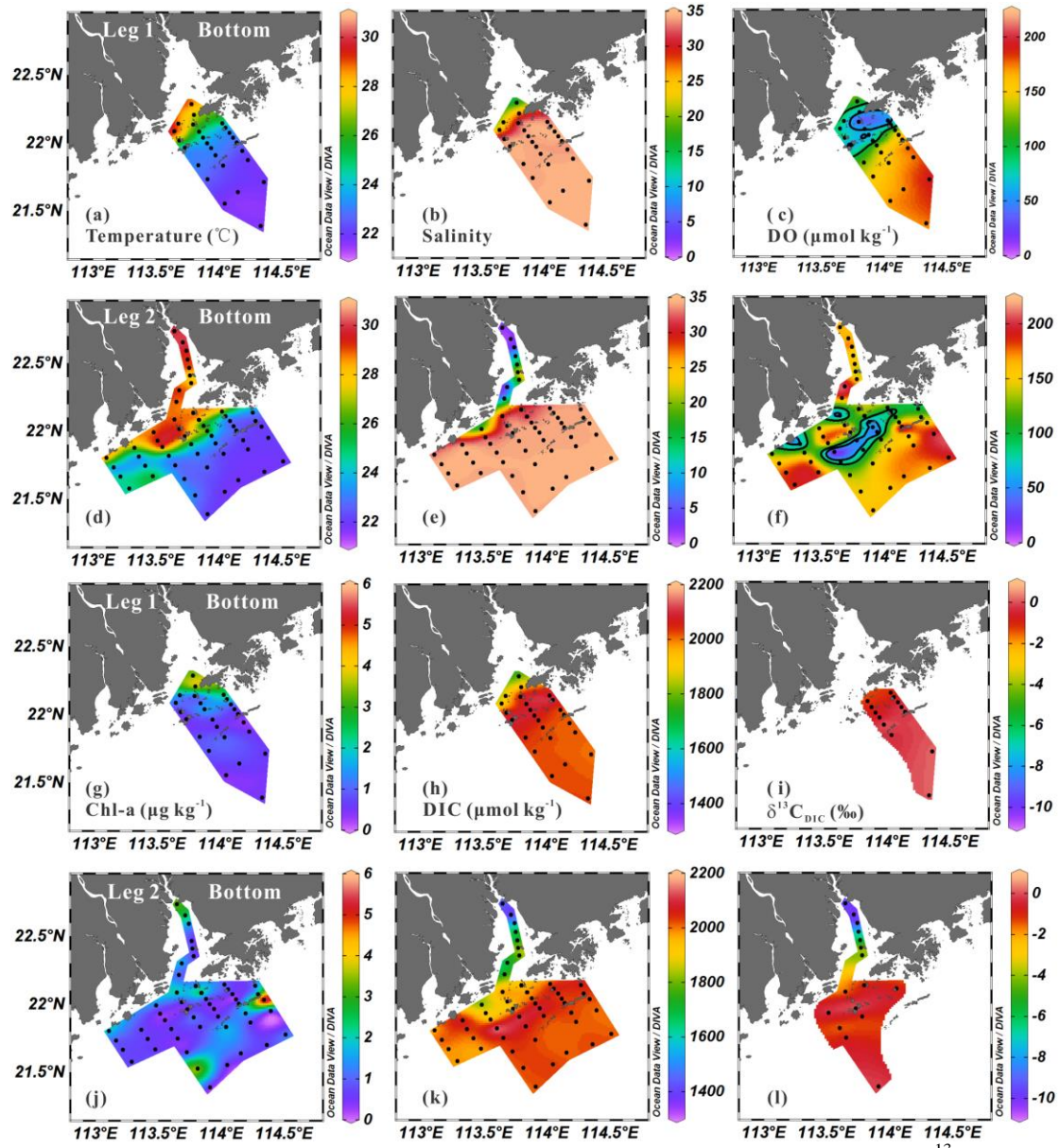
3    Leg 1 stations visited on 13–16 July 2014, and the crosses represent Leg 2 stations visited on

4    19–27 July 2014. Note that the filled diamond is the location of Station A10.

5

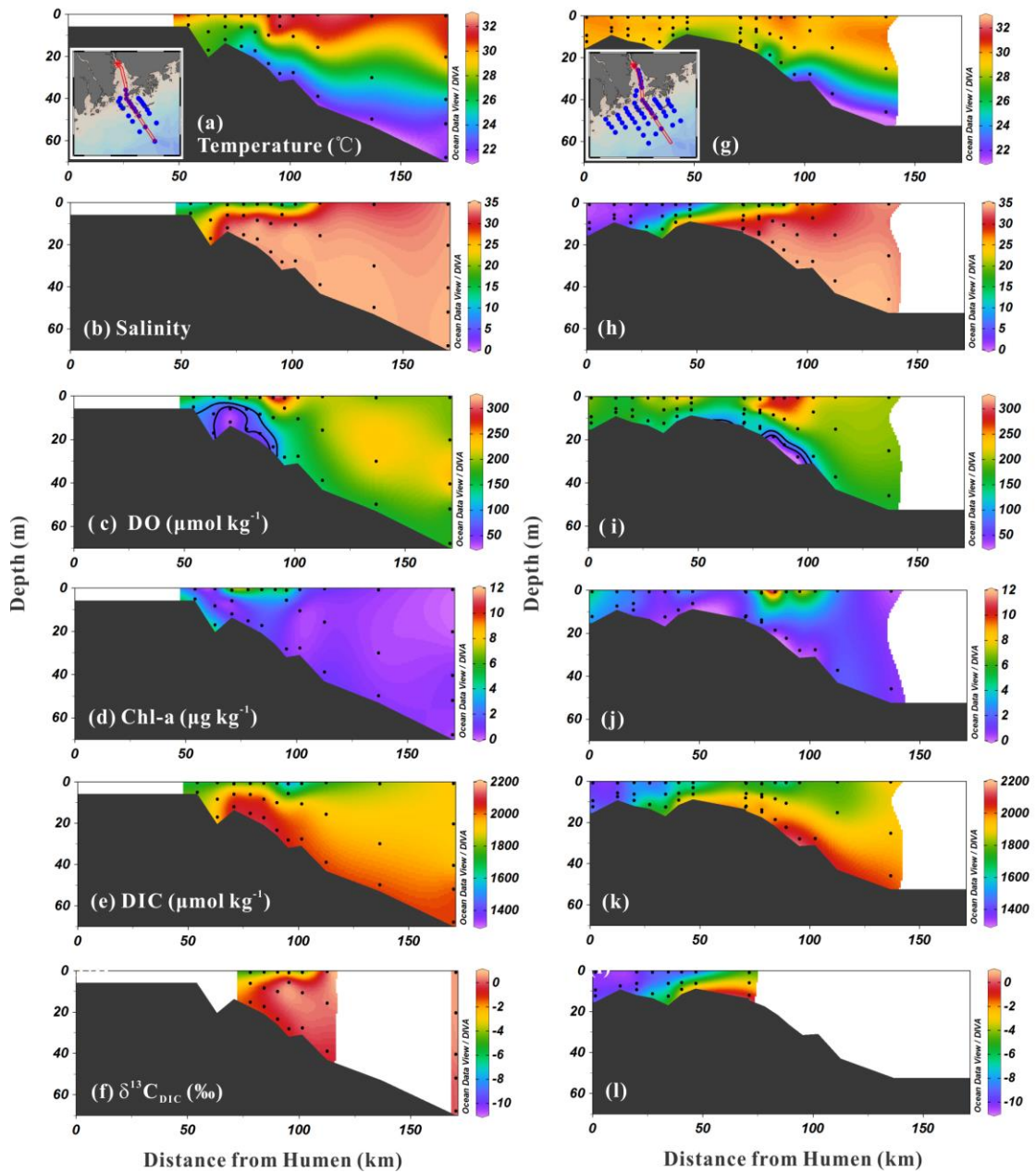


1  
 2 **Figure 2.** Surface water distribution of temperature, salinity, DO, Chl-a, DIC and  $\delta^{13}\text{C}_{\text{DIC}}$   
 3 during Leg 1 (a–c, g–i) and Leg 2 (d–f, j–l).  
 4  
 5  
 6  
 7  
 8



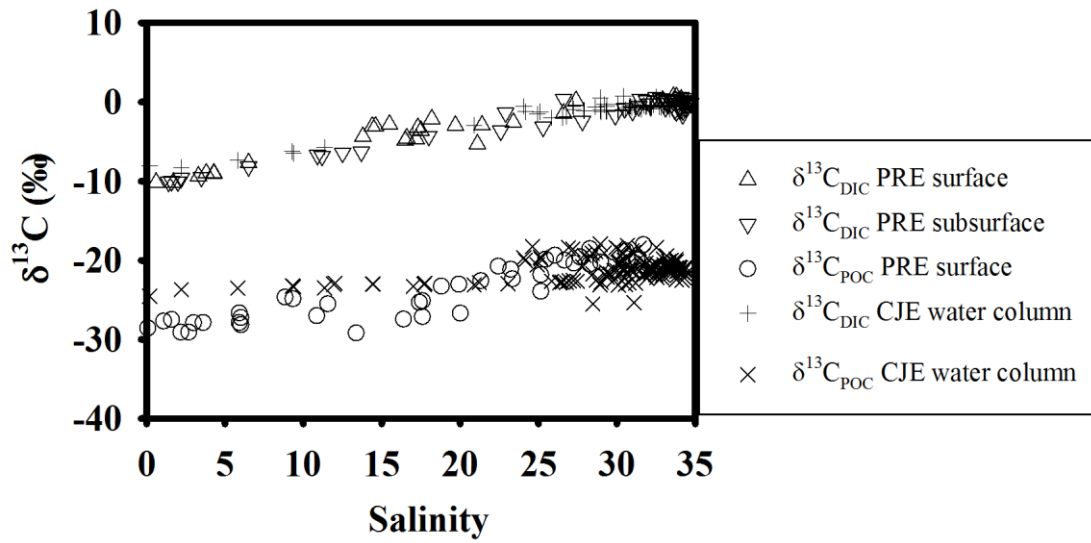
1  
 2 **Figure 3.** Bottom water distribution of temperature, salinity, DO, Chl-a, DIC and  $\delta^{13}\text{C}_{\text{DIC}}$   
 3 during Leg 1 (a–c, g–i) and Leg 2 (d–f, j–l). Note that the black lines in (c) and (f) indicate DO  
 4 contours of 63  $\mu\text{M}$  and 95  $\mu\text{M}$ .

5  
 6  
 7  
 8  
 9  
 10  
 11  
 12  
 13



1 Distance from Humen (km) Distance from Humen (km)  
 2 **Figure 4.** Profiles of temperature, salinity, DO, Chl-a, DIC and  $\delta^{13}\text{C}_{\text{DIC}}$  along Transect A  
 3 during Leg 1 (a–f) and Leg 2 (g–l). Note that the black lines in (c) and (i) indicate DO contours  
 4 of 63  $\mu\text{M}$  and 95  $\mu\text{M}$ .

5  
 6



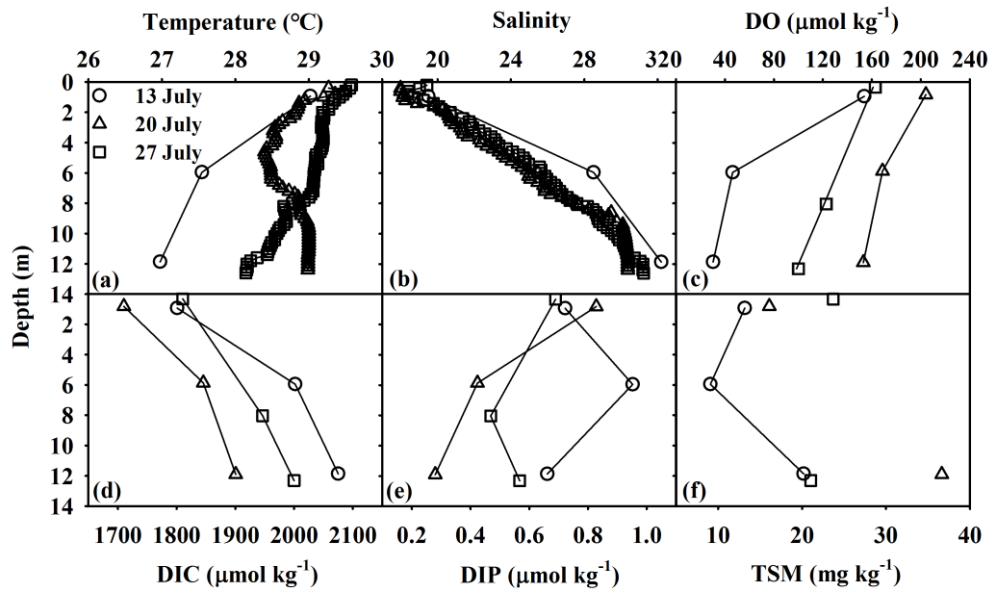
1

2 **Figure 5.** Distribution of  $\delta^{13}\text{C}_{\text{DIC}}$  and  $\delta^{13}\text{C}_{\text{POC}}$  with respect to salinity in the PRE. The up-facing  
 3 and down-facing triangles denote surface and subsurface  $\delta^{13}\text{C}_{\text{DIC}}$  data, respectively, from July  
 4 2014, while the open circles represent  $\delta^{13}\text{C}_{\text{POC}}$  values in surface water from July 2015.  
 5 Additionally, the plus signs and crosses show the  $\delta^{13}\text{C}_{\text{DIC}}$  and  $\delta^{13}\text{C}_{\text{POC}}$  data, respectively, from  
 6 the Changjiang Estuary (CJE) in Wang et al. (2016).

7

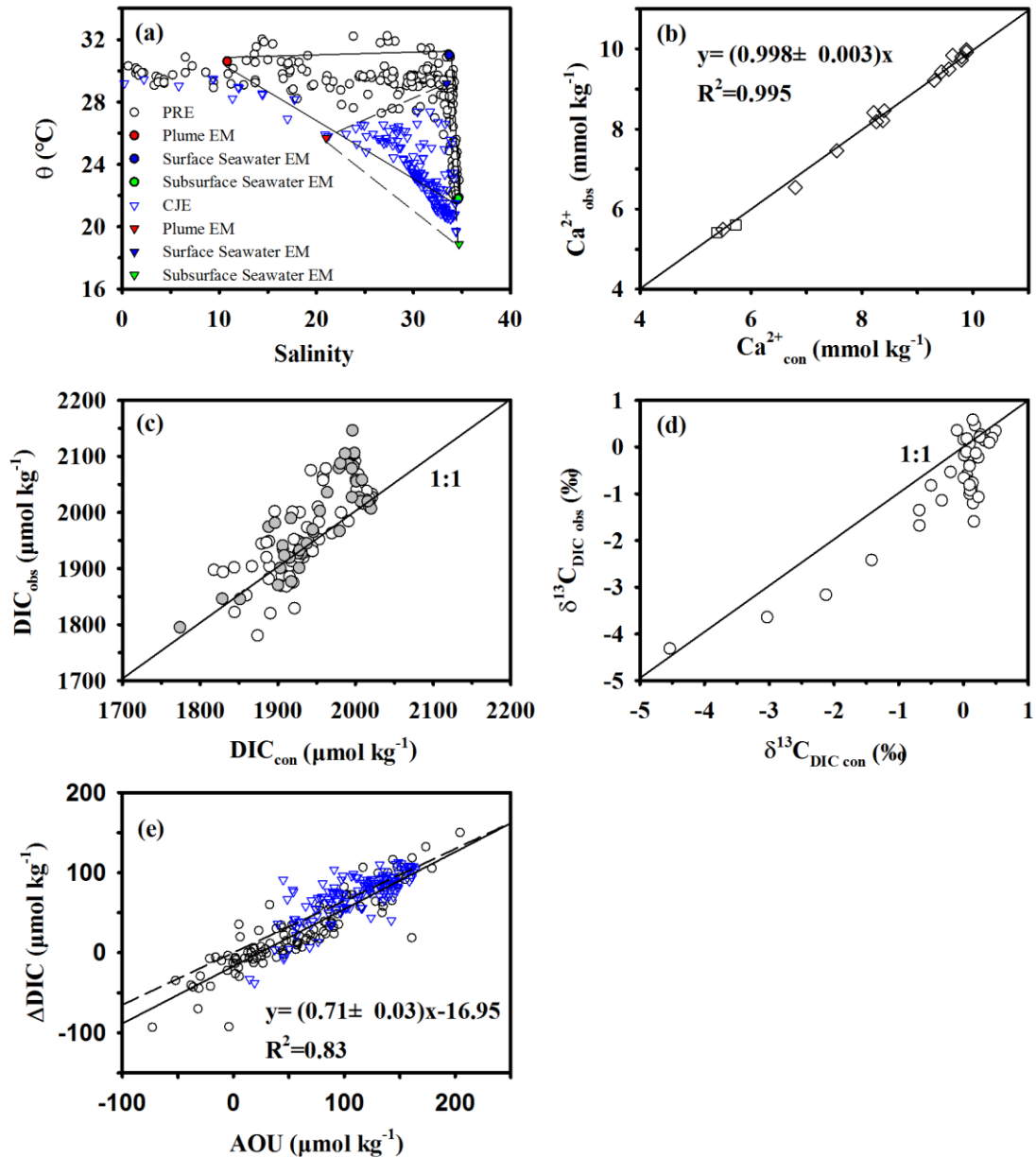


1



2

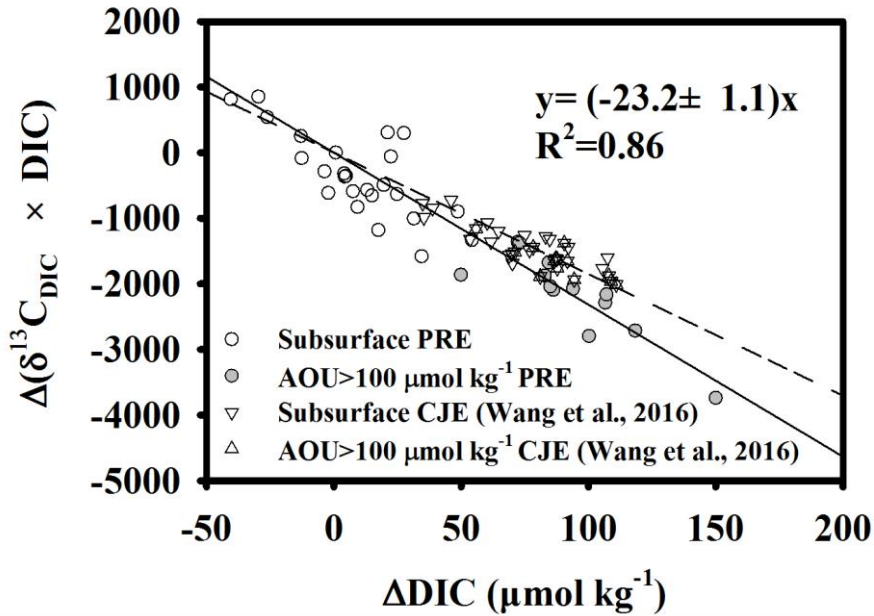
3 **Figure 6.** Profiles of (a) temperature, (b) salinity, (c) DO, (d) DIC, (e) DIP, (f) TSM and their  
4 evolution during repeated sampling at Station A10.



1  
2 **Figure 7.** (a) Potential temperature ( $\theta$ ) ( $^{\circ}\text{C}$ ) vs. salinity in the PRE and adjacent coastal waters  
3 (open circles) based on data collected during the July 2014 cruise. The three end-members are  
4 shown as different coloured symbols. The blue triangles represent data collected during the  
5 August 2011 cruise in the Changjiang Estuary (CJE) (Wang et al., 2016); (b) Correlation  
6 between the field-observed  $\text{Ca}^{2+}$  ( $\text{Ca}^{2+}_{\text{obs}}$ ) and conservative  $\text{Ca}^{2+}$  ( $\text{Ca}^{2+}_{\text{con}}$ ). The straight line  
7 denotes a linear regression line of both surface (square) and subsurface (diamond) data; (c), (d)  
8 Relationship between observed and conservative DIC and  $\delta^{13}\text{C}_{\text{DIC}}$  values. The straight line  
9 represents a 1:1 reference line. Note that the grey dots in Fig. 7c identify data also in Fig. 7d;  
10 and (e) Correlation of  $\Delta\text{DIC}$  vs. AOU for all subsurface water data.  $\Delta\text{DIC}$  is the difference  
11 between the field-observed and conservative DIC concentrations. Also shown is the data from

1 Wang et al. (2016). The straight and dashed lines indicate linear regressions of data from the  
2 PRE and CJE, respectively.

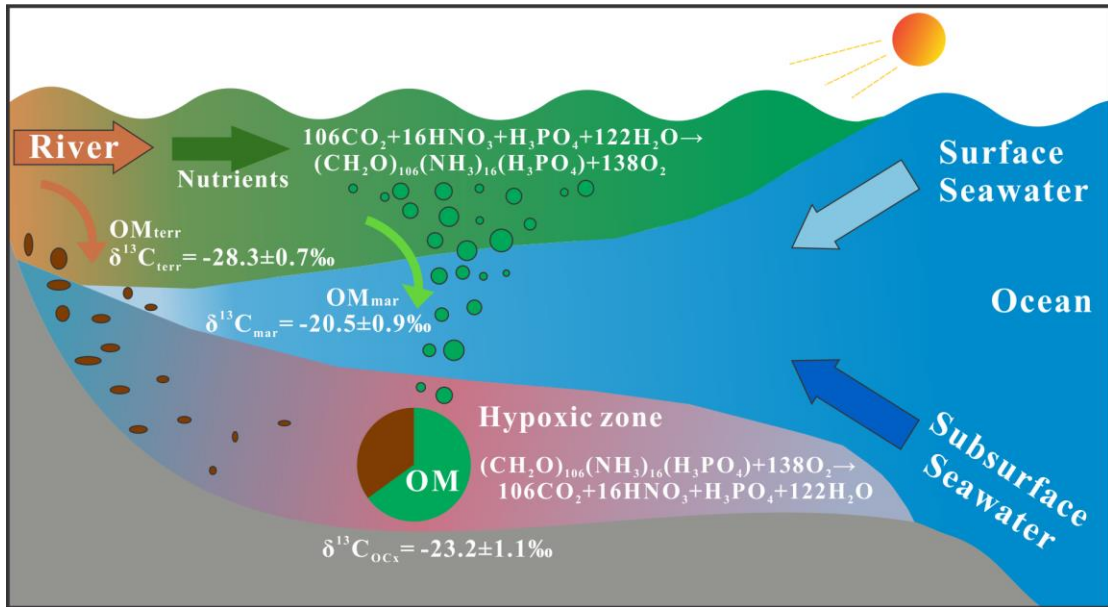
3  
4



5  
6 **Figure 8.**  $\Delta(\delta^{13}\text{C}_{\text{DIC}} \times \text{DIC})$  vs.  $\Delta\text{DIC}$  in the PRE. Samples were collected from subsurface  
7 water (> 5 m). The grey circles represent samples with  $\text{AOU} > 100 \mu\text{mol kg}^{-1}$ .  $\Delta$  is the  
8 difference between the field-observed and conservative values. Also shown is data from the  
9 Changjiang Estuary (CJE) reported by Wang et al. (2016). The straight and dashed lines  
10 indicate linear regression lines of data from the PRE and CJE, respectively.

11





1  
 2 **Figure 9.** A conceptual diagram illustrating the partitioning of oxygen-consuming organic  
 3 matter (OC<sub>mar</sub> vs. OC<sub>terr</sub>) within the hypoxic zone in the lower PRE and the adjacent coastal  
 4 area. See Sect. 5 for explanations.

5